Topological maps and robust Euclidean skeletons in cubical complexes

Michel Couprie
Université Paris-Est, Laboratoire d'informatique Gaspard-Monge, Équipe A3SI, ESIEE Paris, France.
E-mail: m.couprie@esiee.fr

Abstract—In the 90s, several authors introduced the notion of a hierarchic family of 2D Euclidean skeletons, evolving smoothly under the control of a filtering parameter. We provide in this paper a discrete framework which formalizes and generalizes this notion, in particular to higher dimensions. This framework allows us to propose a new skeletonization scheme and to prove several important properties, such as topology preservation and stability w.r.t. parameter changes.

Index Terms—Skeleton, medial axis, topology preservation, topological map, cubical complex, collapse.

INTRODUCTION

Skeleton is one of the most studied and used concepts in pattern recognition and analysis. Since its introduction by H. Blum in the sixties [8], it has been the subject of hundreds of publications dealing with both practical and theoretical aspects. Indeed, despite the simplicity of its most common definition, as the set of all centers of maximal included balls, its use in real applications often raises difficult challenges.

These difficulties are mainly due to two distinct problems.

First, the nice properties of skeleton that can be proved in the continuous framework (uniqueness, thinness, homotopy equivalence, invariance w.r.t. isometries) [25], [22] do not all hold in discrete grids which are commonly used in image processing. Considerable effort has been devoted to design discrete skeletonization methods that aim at retrieving these properties, at least partially. These methods find their roots in different frameworks: discrete geometry [9], [20], [24], [29], [21], digital topology [16], [36], [35], [28], mathematical morphology [30], [33], computational geometry [2], [3], [26], and partial differential equations [32].

Second, even in the continuous framework the skeleton suffers from its sensitivity to small contour perturbations, in other words, its lack of stability. A recent survey [1] summarizes selected relevant studies dealing with this topic. This difficulty can be expressed mathematically: the transformation which associates a shape to its skeleton is only semi-continuous. This fact, among others, explains why it is usually necessary to add a filtering step (or pruning step) to any method that aims at computing the skeleton. Hence, there is a rich literature devoted to skeleton pruning, in which different criteria were proposed in order to discard "spurious" skeleton points or branches: see [4], [26], [3], [24], [2], [34], [21], [5], [15], [23], to cite only a few.

In 2005, F. Chazal and A. Lieutier introduced the λ-medial axis and studied its properties, in particular those related to stability [12]. A major outcome of [12] is the following property: informally, for "regular" values of λ, the λ-medial axis remains stable under perturbations of the shape that are small with regard to the Hausdorff distance. Typical non-regular values are radii of locally largest maximal balls. However, the original definition of the λ-medial axis only holds and make sense in the continuous Euclidean n-dimensional space. In [11], J. Chaussard *et al.* introduced the definition of a discrete λ-medial axis (DLMA) in $\mathbb{Z}^n$.

For certain applications however, the λ-medial axis cannot be used because the desired level of filtering coincides with a non-regular value of λ. When a small modification of the parameter is done around such a value, topological changes or abrupt appearing/disappearing of branches typically occur in the resulting skeketon. For example in Fig. 1, with parameter value $\lambda = 2$, the λ-medial axis contains some spurious branches, and with $\lambda = 3$, an important skeleton branch has disappeared while some spurious branches remain.

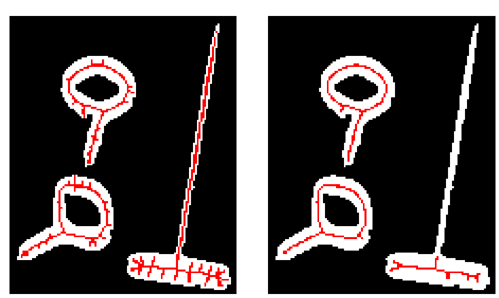

(a) (b)

Fig. 1. (a): A shape and its λ-medial axis, with $\lambda = 2$. (b): Idem, with $\lambda = 3$.

On the other hand, several authors have proposed a general idea that leads to the notion of a family of skeletons, evolving smoothly under the control of a single parameter. They called it hierarchic skeletons [26], veinerization [27] or multiscale skeletons [18]. Such a family of skeletons can be summarized by a function, called potential residual in [26]. The skeletons are obtained as level sets (*i.e.* thresholds) of this function. The method of R.L. Ogniewicz and O. Kübler [26] applies to 2D shapes that are (sets of) planar polygons, and the resulting skeleton is a set of straight line segments which do not necessarily have their extremities on a grid. The authors give a proof that the obtained skeleton is homotopy-equivalent to the original shape, but grid-based discretizations of these skeletons are not guaranteed to share the same property. Veinerization [27] and multiscale skeletons [18] are both methods that operate in the 2D square grid, and that are based on the same general idea. However [27] does not provide an algorithm to compute skeletons in practice, and the algorithm proposed in [18] does not guarantee topology preservation. Extensions of these works to higher-dimensional spaces (*e.g.*, 3D) have not been considered so far, to our knowledge.

In this article, we consider objects that are subsets of an n-dimensional cubic grid, in particular when $n = 2$ or $n = 3$. More precisely, such objects are cubical complexes, that is, they are sets of elements of different dimensions (points, segments, squares, cubes ...) obeying to certain conditions (Sec. 1). We ensure topology preservation by funding our method on the collapse operation, an elementary deformation that preserves the homotopy type (Sec. 2).

We adapt and combine in this framework three ideas: λ-medial axis (Sec. 3), directional parallel thinning, and guided thinning (Sec. 4). This yields a powerful method for building and filtering discrete skeletons. This method also produces a sequence of collapse operations from which we derive an acyclic graph structure that we call a flow graph. Yet, this method is still subject to unstability for non-regular values of parameter λ.

We define, in the framework of cubical complexes, the notion of topological map (based on a flow graph). We prove that if M is a topogical map on an object X, then any level set of M has the same homotopy type as X (Th. 12). Moreover, we prove that if the real numbers a and b are close to each other, then the shapes M_a and M_b (the level sets of M at levels a and b) are close to each other with respect to the Hausdorff distance (Th. 14). This property will assess the stability of our final skeletonization method w.r.t. the parameter value.

Then, we show how to build particular topological maps based on different measures of shape characteristics, thanks to the notion of upstream (Sec. 4, Sec. 7).

Finally, we propose a skeletonization scheme that produces families of filtered homotopic skeletons (Sec. 8). A filtered skeleton is obtained as a level set of the pre-computed topological map. We provide in Sec. 9 some experimental results and comparisons showing that our skeletons are robust w.r.t. rotations, and compare well with other methods of the same class. Unlike former approaches to define and compute hierarchic or multiscale skeletons, our method also applies to 3D objects (Sec. 10).

1 Cubical Complexes

In this section, we recall briefly some basic definitions on cubical complexes, see also [6], [7] for more details. We consider here d-dimensional complexes, mainly with $0 \leqslant d \leqslant 3$.

Let S be a set. If T is a subset of S, we write $T \subseteq S$. We denote by $|S|$ the number of elements of S.

Let $\mathbb{Z}$ be the set of integers. We consider the families of sets $\mathbb{F}^1_0$, $\mathbb{F}^1_1$, such that $\mathbb{F}^1_0 = \{\{a\} \mid a \in \mathbb{Z}\}$, $\mathbb{F}^1_1 = \{\{a, a+1\} \mid a \in \mathbb{Z}\}$. A subset f of $\mathbb{Z}^n$, $n \geqslant 2$, which is the Cartesian product of exactly m elements of $\mathbb{F}^1_1$ and $(n-m)$ elements of $\mathbb{F}^1_0$ is called a *face* or an *m-face* in $\mathbb{Z}^n$, m is the *dimension of* f, we write $\dim(f) = m$.

Observe that any non-empty intersection of faces is a face. For example, the intersection of two 2-faces A and B may be either a 2-face (if $A = B$), a 1-face, a 0-face, or the empty set.

We denote by $\mathbb{F}^n$ the set composed of all faces in $\mathbb{Z}^n$. An m-face is called a *point* if $m = 0$, a *(unit) edge* if $m = 1$, a *(unit) square* if $m = 2$, a *(unit) cube* if $m = 3$.

Let f be a face in $\mathbb{F}^n$. We set $\hat{f} = \{g \in \mathbb{F}^n \mid g \subseteq f\}$ and $\hat{f}^* = \hat{f} \setminus \{f\}$.
Any $g \in \hat{f}$ is called a *face of* f.
We call *star of* f the set $\check{f} = \{g \in \mathbb{F}^n \mid f \subseteq g\}$, and we write $\check{f}^* = \check{f} \setminus \{f\}$: any element of $\check{f}$ is a *coface of* f. It is plain that $g \in \hat{f}$ iff $f \in \check{g}$.
If X is a finite set of faces in $\mathbb{F}^n$, we write $X^- = \bigcup\{\hat{f} \mid f \in X\}$, X^- is the *closure of* X.

A finite set X of faces in $\mathbb{F}^n$ is a *complex (in $\mathbb{F}^n$)* if $X = X^-$. See in Fig. 2d an example of a complex, and in Fig. 2b,c examples of sets of faces that are not complexes.

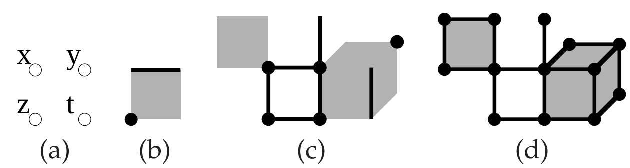

Fig. 2. (a): Four points in $\mathbb{Z}^2$: $x = (0,1)$; $y = (1,1)$; $z = (0,0)$; $t = (1,0)$. (b): A graphical representation of the set of faces $\{f_0, f_1, f_2\}$, where $f_0 = \{z\} = \{0\} \times \{0\}$ (a 0-face), $f_1 = \{x, y\} = \{0,1\} \times \{1\}$ (a 1-face), and $f_2 = \{x, y, z, t\} = \{0,1\} \times \{0,1\}$ (a 2-face). (c): A set of faces X, which is not a complex. (d): The set X^-, *i.e.* the closure of X, which is a complex.

2 Collapse

The *collapse operation* is an elementary topology-preserving transformation which has been introduced by J.H.C. Whitehead [37] and plays an important role in combinatorial topology, it can be seen as a discrete analogue of a continuous deformation (a retraction). Collapse is known to preserve the homotopy type.

Let X be a complex in $\mathbb{F}^n$ and let $(f,g) \in X^2$. If f is the only face of X that strictly includes g, then g is said to be *free for* X and the pair (f,g) is said to be a *free pair for* X. In other terms, (f,g) is a free pair for X whenever $\check{g}^* \cap X = \{f\}$. Notice that, if (f,g) is a free pair, then we have necessarily $\dim(g) = \dim(f) - 1$.

Let X be a complex, and let (f,g) be a free pair for X. Let $m = \dim(f)$. The complex $X \setminus \{f,g\}$ is an *elementary collapse of* X, or an *elementary* m*-collapse of* X.
Let X, Y be two complexes. We say that X *collapses onto* Y, and we write $X \searrow Y$, if $Y = X$ or if there exists a *collapse sequence from* X *to* Y, *i.e.*, a sequence of complexes $\langle X_0, ..., X_\ell \rangle$ such that $X_0 = X$, $X_\ell = Y$, and X_i is an elementary collapse of X_{i-1}, for each $i \in \{1,\ldots,\ell\}$. See Fig. 3 for an illustration. Let $J = \langle (f_i, g_i) \rangle_{i=1}^{\ell}$ be the sequence of pairs of faces of X such that $X_i = X_{i-1} \setminus \{f_i, g_i\}$, for any $i \in [1,\ell]$. We also call the sequence J a *collapse sequence (from* X *to* Y*)*.

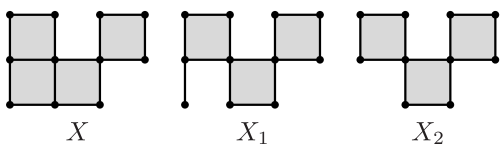

Fig. 3. X: a 2-dimensional complex. X_1: a complex such that X collapses onto X_1; a free pair composed of a square and an edge has been removed. X_2: a complex such that X_1 collapses onto X_2; (a free pair composed of an edge and a vertex has been removed), hence X collapses onto X_2.

Let us now state an elementary property of collapse, which gives a necessary and sufficient condition under which two collapse operations may be performed in parallel (or in any order) while preserving topology.

Proposition 1. *Let X be a complex, and let (f,g) and (k,ℓ) be two distinct free pairs for X. The complex X collapses onto $X \setminus \{f,g,k,\ell\}$ if and only if $f \neq k$. In this case, $\langle (f,g),(k,\ell) \rangle$ and $\langle (k,\ell),(f,g) \rangle$ are both collapse sequences from X.*

Proof. If $f = k$, then it is plain that (k,ℓ) is not a free pair for $Y = X \setminus \{f,g\}$ as $k = f \notin Y$. Also, (f,g) is not free for $X \setminus \{k,\ell\}$. If $f \neq k$, then we have $g \neq \ell$, $\check{g}^* \cap X = \{f\}$ (g is free for X) and $\check{\ell}^* \cap X = \{k\}$ (ℓ is free for X). Thus, we have $\check{\ell}^* \cap Y = \{k\}$ as $\ell \neq g$ and $k \neq f$. Therefore, (k,ℓ) is a free pair for Y. The same reasonning shows that (f,g) is a free pair for $Y' = X \setminus \{k,\ell\}$. □

From Prop. 1, the following corollary is immediate.

Corollary 2. *Let X be a complex, and let $(f_1,g_1)\ldots(f_m,g_m)$ be m distinct free pairs for X such that, for all $a,b \in \{1,\ldots,m\}$ (with $a \neq b$), $f_a \neq f_b$. The complex X collapses onto $X \setminus \{f_1, g_1 \ldots f_m, g_m\}$.*

The corollary (Cor. 4) of the following property will be useful in the sequel.

Proposition 3. *Let $J = \langle (f_i,g_i) \rangle_{i=1}^{\ell}$ be a collapse sequence from a complex X to a complex Y. Let $j \in \{2,\ldots,\ell\}$ such that (f_j,g_j) is free for X. Let J' denote the sequence obtained from J by swapping pairs $j-1$ and j, more precisely, $J' = \langle (f'_i,g'_i) \rangle_{i=1}^{\ell}$ with $f'_j = f_{j-1}, g'_j = g_{j-1}$, $f'_{j-1} = f_j, g'_{j-1} = g_j$, and for all $i \in \{1,\ldots,\ell\} \setminus \{j,j-1\}$, $f'_i = f_i$ and $g'_i = g_i$. Then, the sequence J' is also a collapse sequence from X to Y.*

Proof. We set $X'_i = X'_{i-1} \setminus \{f'_i, g'_i\}$ and $X_i = X_{i-1} \setminus \{f_i, g_i\}$, for all $i \in \{1,\ldots,\ell\}$, and $X'_0 = X_0 = X$. Obviously, we have $X'_i = X_i$ for all $i \in \{0,\ldots,\ell\} \setminus \{j-1\}$, thus we only have to prove $X_{j-2} \searrow X'_{j-1} \searrow X_j$. We know that (f_{j-1}, g_{j-1}) is free for X_{j-2} (since J is a collapse sequence), and that (f_j,g_j) is free for X_{j-2} (since it free for X), hence $X_{j-2} \searrow X'_{j-1}$. Furthermore, $f_{j-1} \neq f_j$ because both pairs are in the collapse sequence J. By Prop. 1, we deduce that (f_{j-1}, g_{j-1}) is free for $X_{j-2} \setminus \{f_j, g_j\} = X'_{j-1}$, hence $X'_{j-1} \searrow X_j$. □

Corollary 4. *Let $J = \langle (f_i,g_i) \rangle_{i=1}^{\ell}$ be a collapse sequence from a complex X to a complex Y. Let $j_1,\ldots,j_k \in \{1,\ldots,\ell\}$ be distinct indices such that (f_{j_i}, g_{j_i}) is free for X for any $i \in \{1,\ldots,k\}$. Let J' denote the sequence obtained from J by shifting pairs j_i to the beginning of the sequence, more precisely, $J' = \langle (f'_i,g'_i) \rangle_{i=1}^{\ell}$ with $f'_i = f_{j_i}, g'_i = g_{j_i}$ for all $i \in \{1,\ldots,k\}$, and the other pairs of J' are the remaining pairs of J left in the same order. Then, the sequence J' is also a collapse sequence from X to Y.*

3 The discrete λ-medial axis and the projection radius (PR) map

The original definition of the λ-medial axis (see [12]) holds and makes sense in the continuous Euclidean n-dimensional space. The definition of a discrete λ-medial axis (DLMA) in $\mathbb{Z}^n$ is given in [11], together with an experimental evaluation of its stability and rotation invariance.

Notice that the DLMA applies on a binary image (*i.e.*, a set of voxels or a subset of $\mathbb{Z}^3$), not on a complex. However, the straightforward correspondance between voxels in $\mathbb{Z}^3$ and 3-faces in $\mathbb{F}^3$ allows us to use the DLMA and related notions in the context of cubical complexes.

Let $x, y \in \mathbb{R}^n$, we denote by $d(x,y)$ the Euclidean distance between x and y, in other words, $d(x,y) = (\sum_{k=1}^{n}(y_k - x_k)^2)^{\frac{1}{2}}$. Let $S \subseteq \mathbb{R}^n$, we set $d(y,S) = \min_{x \in S}\{d(y,x)\}$.

Let $x \in \mathbb{R}^n, r \in \mathbb{R}^+$, we denote by $B_r(x)$ the *ball of radius* r *centered on* x, defined by $B_r(x) = \{y \in \mathbb{R}^n \mid d(x,y) \leqslant r\}$.

Let S be a nonempty subset of $\mathbb{R}^n$, and let $x \in \mathbb{R}^n$. The *projection of* x *on* S, denoted by $\Pi_S(x)$, is the set of points y of S which are at minimal distance from x ; more precisely,

$$\Pi_S(x) = \{y \in S \mid \forall z \in S, d(y,x) \leqslant d(z,x)\}.$$

Let X be an open bounded subset of $\mathbb{R}^n$, and let $\lambda \in \mathbb{R}^+$. The λ*-medial axis of* X is the set of points x in X such that the radius of the smallest ball that includes $\Pi_{\overline{X}}(x)$ is not less than λ (see Fig. 4).

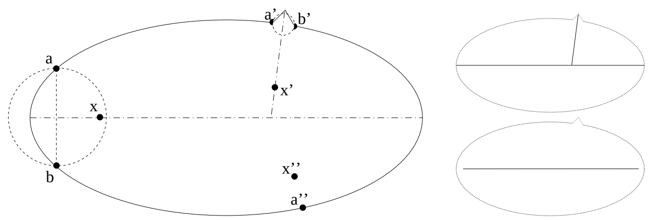

Fig. 4. Illustration of the λ-medial axis. Left: Points x, x' and x'' and their respective closest boundary points. Top right: λ-medial axis with $\lambda = \epsilon$, a very small positive real number. Bottom right: λ-medial axis with $\lambda = d(a', b') + \epsilon$.

For each point $x \in \mathbb{Z}^n$, we define the *direct neighborhood of* x as $N(x) = \{y \in \mathbb{Z}^n \mid d(x, y) \leqslant 1\}$.

Transposing directly the definition of the λ-medial axis to the discrete grid $\mathbb{Z}^n$ would yield unsatisfactory results (see [11]), this is why we need the following notion. Let $S \subseteq \mathbb{Z}^n$, and let $x \in S$. The *extended projection of* x *on* $\overline{S}$, denoted by $\Pi^e_{\overline{S}}(x)$, is the union of the sets $\Pi_{\overline{S}}(y)$, for all y in $N(x)$ such that $d(y, \overline{S}) \leqslant d(x, \overline{S})$.

Let S be a finite subset of $\mathbb{Z}^n$, and let $\lambda \in \mathbb{R}^+$. We define the function PR_S which associates, to each point x of S, the value $PR_S(x)$ that is the radius of the smallest ball enclosing all the points of the extended projection of x on $\overline{S}$. In other terms, $PR_S(x) = \min\{r \in \mathbb{R} \mid \exists y \in \mathbb{R}^n, B_r(y) \supseteq \Pi^e_{\overline{S}}(x)\}$, and we call $PR_S(x)$ the *projection radius of* x *(for* S*)*. The *discrete* λ*-medial axis of* S, denoted by $DLMA(S, \lambda)$, is the set of points x in S such that $PR_S(x) \geqslant \lambda$.

In Fig. 5, we show the function PR_S and three examples of DLMAs of a shape S. Note that the function PR_S can be computed once and stored as a grayscale image, and that any DLMA of S is a level set of this function at a particular value λ. Notice also that DLMA has not, in general, the same topology as the original shape. For more details, illustrations and performance analysis, see [11].

4 Guided collapse and flow graph

In this section we introduce a thinning scheme that produces a collapse sequence, based on an arbitrary priority map (*e.g.*, a distance map or a projection radius map). The general idea of guided thinning is not new: it has been used by several authors to produce skeletons based on the Euclidean distance [16], [36], [35], [28], and consists of using the priority function in order to specify which elements must be considered at each step of the thinning. Here, we combine this general idea with a parallel directional collapse algorithm introduced in [10], in order to minimize the number of arbitrary decisions. When several elements share the same priority, which may occur quite often, we remove in parallel all such elements that satisfy a condition based on direction and dimension. All directions and dimensions are successively explored.

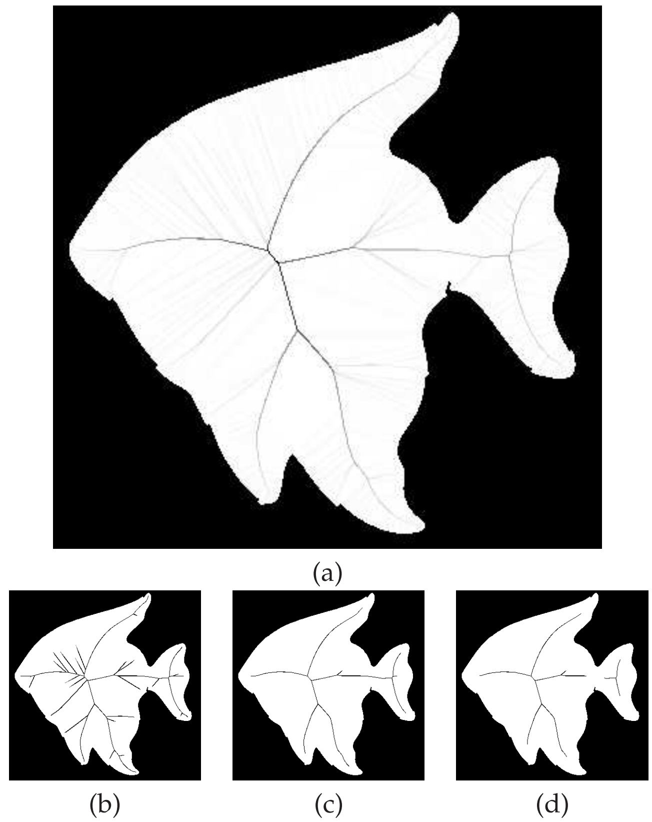

Fig. 5. (a): The function PR_S superimposed to the shape S. Darkest colors represent highest values of $PR_S(x)$. Any DLMA of S is a level set of this function at a particular value λ. (b,c,d): Discrete $lambda$-medial axis with $\lambda = 10, 30, 45$ respectively.

First, we need to define the *direction* and the *orientation* of a free face.

Let $f \in \mathbb{F}^n$, the *center of* f is the center of mass of the points in f, that is, $c_f = \frac{1}{|f|}\sum_{a \in f} a$. The center of f is an element of $[\frac{\mathbb{Z}}{2}]^n$, where $\frac{\mathbb{Z}}{2}$ denotes the set of half integers. Notice that $\mathbb{Z} \subset \frac{\mathbb{Z}}{2}$, as any z is half $2z$. Let $X \preceq \mathbb{F}^n$, let (f, g) be a free pair for X, and let c_f and c_g be the respective centers of the faces f and g. We denote by $V(f, g)$ the vector $(c_f - c_g)$ of $[\frac{\mathbb{Z}}{2}]^n$.

Let (f, g) be a free pair, the vector $V(f, g)$ has only one non-null coordinate. We define $Dir(f, g)$ as the index of the non-null coordinate of $V(f, g)$. Thus, $Dir()$ is a surjective function from $\mathbb{F}^n \times \mathbb{F}^n$ to $\{1, \ldots, n\}$ such that, for all free pairs (f, g) and (i, j) for X, $Dir(f, g) = Dir(i, j)$ if and only if $V(f, g)$ and $V(i, j)$ are collinear. The number $Dir(f, g)$ is called the *direction* of the free pair (f, g). The free pair (f, g) has a *positive orientation*, and we write $Orient(f, g) = 1$, if the non-null coordinate of $V(f, g)$ is positive; otherwise (f, g) has a *negative orientation*, and we write $Orient(f, g) = 0$.

Considering two distinct free pairs (f, g) and (i, j) for $X \preceq \mathbb{F}^n$ such that $Dir(f, g) = Dir(i, j)$ and $Orient(f, g) = Orient(i, j)$, we have $f \neq i$. From this observation and Cor. 2, we deduce the following property.

Corollary 5. *Let $X \preceq \mathbb{F}^n$, and let $(f_1, g_1), \ldots, (f_m, g_m)$ be m distinct free pairs for X having all the same direction and the same orientation. The complex X collapses onto $X \setminus \{f_1, g_1, \ldots, f_m, g_m\}$.*

Now, we are ready to introduce algorithm 1. Thanks to Cor. 5, we have the following property.

Corollary 6. *Whatever the complex X and the map P from X to $\mathbb{R}$, X collapses onto GuidedCollapse(X, P).*

Algorithm 1: *GuidedCollapse*(X, P)

Data: A cubical complex $X \preceq \mathbb{F}^n$, and a map P from X to $\mathbb{R}$ (priority map)

$J = \langle\rangle$;
$R = \{(p, f, g) \mid (f, g)$ is free for X, $p = \max(P(f), P(g))\}$;
while $R \neq \emptyset$ **do**
    $m = \min\{p \mid (p, ., .) \in R\}$; $Q = \{(m, ., .) \in R\}$;
    $R = R \setminus Q$;
    $L = \{(f, g) \mid (., f, g) \in Q\}$;
    for $t = 1 \to n$ **do**
        for $s = 0 \to 1$ **do**
            for $d = n \to 1$ **do**
                $T = \{(f, g) \in L \mid (f, g)$ is free for X, *Dir*$(f, g) = t$, *Orient*$(f, g) = s$, $\dim(f) = d\}$;
                $X = X \setminus T$;
                foreach $(f, g) \in T$ **do** $J = J + (f, g)$;
                foreach $(i, j) \in X^2, j \in \hat{f}^*$ **do**
                    if (i, j) *is free for* X **then**
                        $p = \max(P(i), P(j))$;
                        if $p \leqslant m$ **then** $L = L \cup \{(i, j)\}$;
                        $R = R \cup \{(p, i, j)\}$;
return J;

Algorithm *GuidedCollapse* may be implemented to run in $O(N \log N)$ time complexity, where n denotes the cardinality of X, using a balanced binary tree data structure (see [14]) for representing the set R.

To conclude this section, we introduce the notion of a flow graph associated to a given collapse sequence.

A *(finite directed) graph* is a pair (V, E) where V is a finite set and E is a subset of $V \times V$. An element of V is called a *vertex*, an element of E is called an *arc*. A *path in* (V, E) is a sequence $\langle v_i \rangle_{i=0}^{\ell}$ of vertices such that for all $i \in \{1, \ldots, \ell\}$, we have $(v_{i-1}, v_i) \in E$. The number ℓ is the *length* of the path. If $\ell = 0$ the path is said *trivial*. If $v_0 = v_\ell$ the path is a *cycle*. The graph is *acyclic* if it does not contain any non-trivial cycle.

Definition 7. *Let X be a complex and $J = \langle (f_i, g_i) \rangle_{i=1}^{\ell}$ be a collapse sequence from X. For any $k \in \{1, \ldots, \ell\}$, we set $X_k = X \setminus \{f_i, g_i\}_{i=1}^{k}$, and $X_0 = X$. We set $E_1 = \{(g_i, f_i)\}_{i=1}^{\ell}$ and $E_2 = \bigcup_{k=1}^{\ell} \{(f_k, g) \mid g \in \hat{f_k}^* \cap X_k\}$. The* flow graph *associated to J is the (directed) graph whose vertex set is X and whose edge set is $E = E_1 \cup E_2$.*

This definition is illustrated in Fig. 6.

It can be easily seen that, whatever the complex X and the collapse sequence J from X, the flow graph associated to J is acyclic.

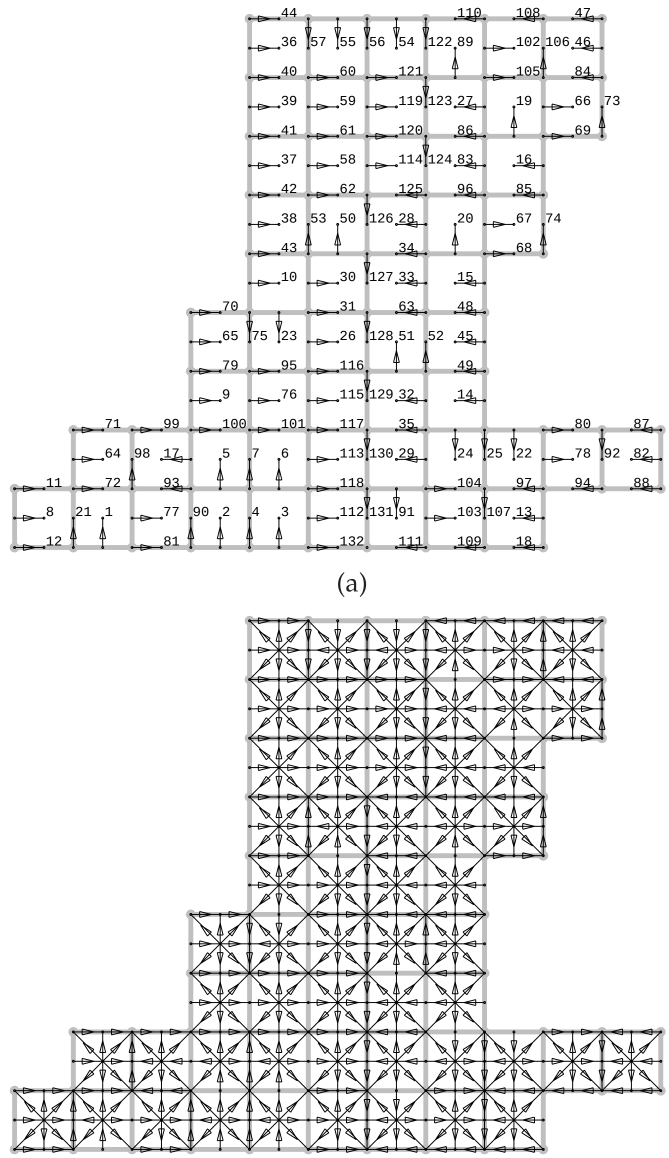

(a)

(b)

Fig. 6. (a): A collapse sequence J. Each pair (f_i, g_i) of J is depicted by an arrow from g_i to f_i. The numbers indicate the indices of the pairs in J. (b): The flow graph associated to J.

In Fig. 7 we illustrate flow graphs associated with collapse sequences that were obtained by the above algorithm using two different priority maps. For the sake of readability, we only display a spanning directed forest (which is a tree, in this case) extracted from the flow graph. For Fig. 7d, the priority map is the Euclidean distance map displayed in Fig. 7b, and for Fig. 7e, the priority map is the projection radius map displayed in Fig. 7c. We observe that each branch of a λ-medial axis (level set of Fig. 7c) corresponds, roughly speaking, to a path in the flow graph Fig. 7e, but this is not true if we consider the flow graph Fig. 7d.

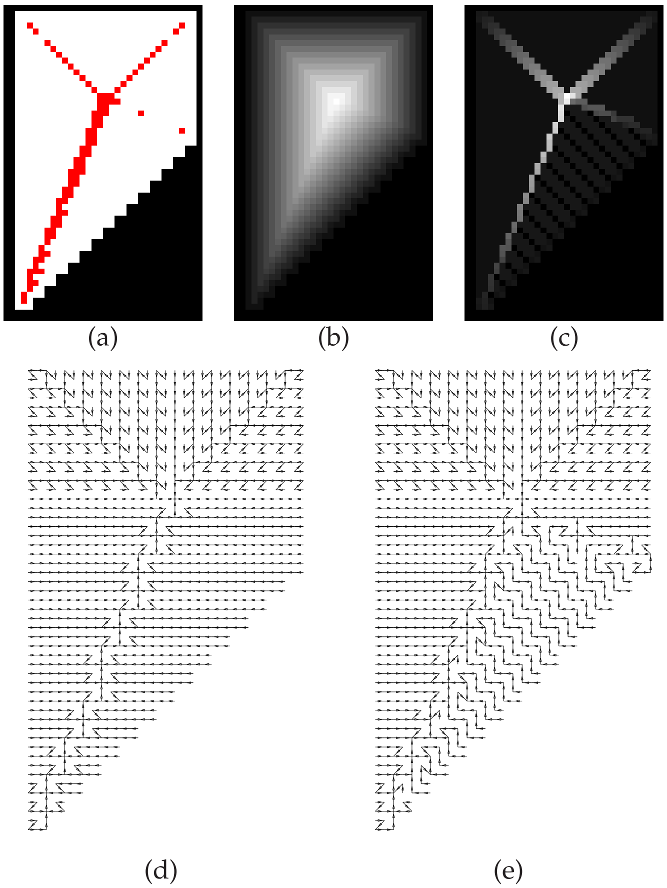

Fig. 7. (a): Original object X (complex). Superimposed: centers of maximal included Euclidean balls. (b): Euclidean distance map of X (named ED). (c): Projection radius map of X (named PR). (d): Spanning forest extracted from the flow graph associated to the sequence *GuidedCollapse*(X, ED). (e): Spanning forest extracted from the flow graph associated to the sequence *GuidedCollapse*(X, PR).

5 Upstream of a vertex and its valuation

From now, we consider a collapse sequence $J = \langle (f_i, g_i) \rangle_{i=1}^{\ell}$ from a complex X, and its associated flow graph $(X, E = E_1 \cup E_2)$. Using the notations of Def. 7, any pair (f_k, g_k) of J is free for X_{k-1}, and we have $X = X_0 \searrow \ldots \searrow X_\ell$. We define $F = \{f_i\}_{i=1}^{\ell}$, $G = \{g_i\}_{i=1}^{\ell}$ and $X_J = F \cup G$.

Let $x \in X$, we denote by $\Gamma(x)$ the set of *successors of* x in the acyclic graph (X, E), that is, $\Gamma(x) = \{y \in X \mid (x, y) \in E\}$, and we denote by $\Gamma^{-1}(x)$ the set of *predecessors of* x in this graph, that is, $\Gamma^{-1}(x) = \{y \in X \mid (y, x) \in E\}$. We denote by $d^+(x)$ the *outer degree* of the vertex x in the graph (X, E), that is, the number of successors of x.

We call *upstream of* x the set of all vertices that are ancestors of x in the flow graph, that is, the set $U(x) = \{y \in X \mid$ there is a path from y to x in $(X, E)\}$.

In a collapse sequence, certain pairs can be swapped or eliminated, yielding another collapse sequence (see *e.g.* Cor. 4). Intuitively, the elements of the upstream of a face x of X are those that must indeed be collapsed before x can itself collapse. In Fig. 8 we show several examples of vertices and their upstream.

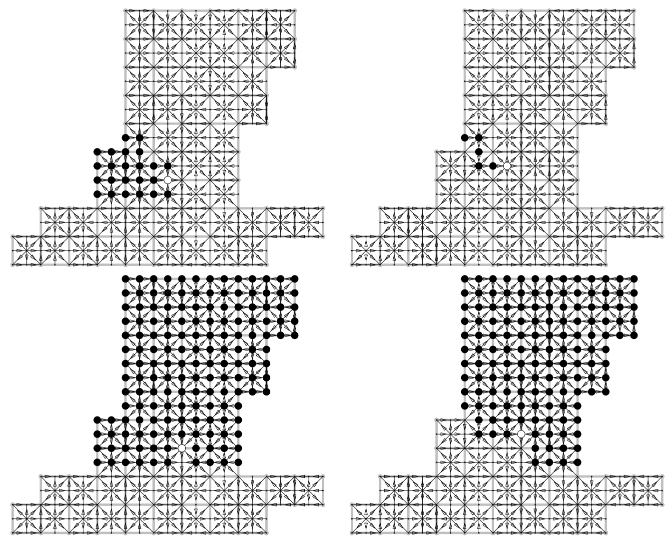

Fig. 8. Four vertices (white discs) and their respective upstreams (black discs), for the same flow graph as in Fig. 6.

Let L be a map from X to $\mathbb{R} \cup \{+\infty\}$. Roughly speaking, the map $\widetilde{L}$ defined below cumulates, for each vertex x, the values of L on all vertices of the upstream of x.

Definition 8. *Let L be a map from X to $\mathbb{R} \cup \{+\infty\}$. We define the map $\widetilde{L}$ such that, for any $x \in X$:*

$$\widetilde{L}(x) = L(x) + \sum_{y \in \Gamma^{-1}(x)} \widetilde{L}(y)/d^+(y)$$

Notice that this definition is recursive, and that it makes sense since the graph (X, E) is acyclic. The values $\widetilde{L}(x)$ can be computed thanks to the following recursive program (algorithm 3) that has a linear time complexity.

Algorithm 2: *IntegrateRec*$(X, \Gamma, \Gamma^{-1}, L, R, x)$

```
if R(x) ≠ −∞ then return R(x);
S = L(x);
foreach y ∈ Γ^{-1}(x) do
    S = S + (IntegrateRec(X, Γ, Γ^{-1}, L, R, y)/|Γ(y)|);
R(x) = S;
return R(x);
```

Algorithm 3: *Integrate*$(X, \Gamma, \Gamma^{-1}, L)$

Data: X: a cubical complex; Γ, Γ^{-1}: the successor and the predecessor function of a directed acyclic graph on X; L: a map from X to $\mathbb{R}$;
Result: R: a map from X to $\mathbb{R}$
foreach $x \in X$ **do** $R(x) = -\infty$;
foreach $x \in X$ **do** *IntegrateRec*$(X, \Gamma, \Gamma^{-1}, L, R, x)$;
return R;

Two particularly simple functions L yield meaningful indicators associated to the elements of X. Let us first consider $L_1 = 1_X$, the constant unity function on X. The map $\widetilde{L}_1$ associates, to each element x of X, the "area of $U(x)$" (or its volume in 3D). Now, let us consider $L_2 = 1_{B(X)}$, where $B(X)$ is the set of all faces that are free for X, and all faces included in these faces. We call $B(X)$ the *border of* X. In other words, $L_2(x) = 1$ if $x \in B(X)$, and $L_2(x) = 0$ otherwise. The map $\widetilde{L}_2$ associates, to each element x of X, a measure (length in 2D, surface area in 3D) of $U(x) \cap B(X)$.

Fig. 9(a_1, a_2) show the maps $L_1 = 1_Y$ and $L_2 = 1_{B(Y)}$ respectively, for the same object Y. The maps $\widetilde{L}_1$ and $\widetilde{L}_2$ are displayed in Fig. 9(b_1, b_2).

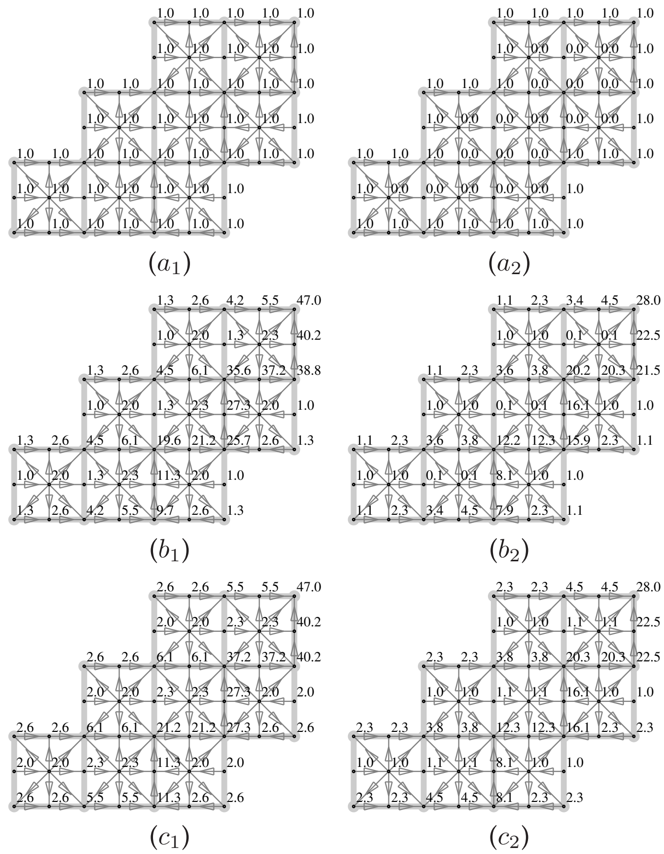

Fig. 9. (a_1, a_2): Maps $L_1 = 1_Y$ and $L_2 = 1_{B(Y)}$ on the same complex Y. (b_1, b_2): Maps $\widetilde{L}_1$ and $\widetilde{L}_2$. For the sake of readability, only one digit after the decimal point is displayed. (c_1, c_2): Results S_1 and S_2 of the *AlphaTM* operator on $\widetilde{L}_1$ and $\widetilde{L}_2$, respectively, with $\alpha = 0.1$.

6 TOPOLOGICAL MAPS

In this section, we introduce the notion of topological map. A topological map is a map on the vertices of X that satisfies certain conditions relative to a collapse sequence J and its associated flow graph. Then, we prove an important property of such maps: if M is a topological map, then any level set of M is homotopy-equivalent to X. In Sec. 7, we will show how to build such a map, based on any given function on X.

Definition 9. *Let M be a map from X to $\mathbb{R} \cup \{+\infty\}$. We say that M is a* topological map on X (based on J) *if:*
i) for all (g, f) in E_1, $M(g) = M(f)$; and
ii) for all (f, g) in E_2, $M(g) > M(f)$; and
iii) for all g in $X \setminus X_J$, $M(g) = +\infty$.

Let α be a strictly positive real number. If we replace ii) with the stronger requirement:
ii') for all (f, g) in E_2, $M(g) \geqslant M(f) + \alpha$,
*then we say that M is an α-*topological map on X (based on J).

The notion of topological map is inspired from the one of discrete Morse function (see [19]). A topological map can be seen (apart from the infinite values) as a particular case of discrete Morse function, and Th. 12 could also be proved using results of [19]. However as the proof is short we include it for the sake of self-containedness.

Let $\lambda \in \mathbb{R} \cup \{+\infty\}$, we define $M_\lambda = \{x \in X \mid M(x) \geqslant \lambda\}$, the *(upper) level set of M at level λ*. The main property of a topological map M is that any level set of M is homotopy-equivalent to X, as implied by the following theorem (Th. 12, see Fig. 11 for an illustration). The two next propositions will be used for proving it.

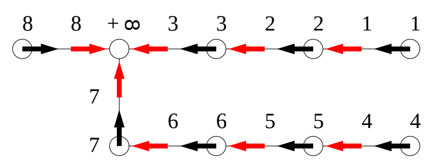

Fig. 10. A 1-complex X, a flow graph on X (black arrows for arcs of E_1, red arrows for arcs of E_2), and a (1-)topological map M on X (numbers).

Proposition 10. *Let $(g_k, f_k) \in E_1$. For all g' in $\hat{f_k}^*$ such that $g' \neq g_k$, we have $(f_k, g') \in E_2$.*

Proof. We know that (f_k, g_k) is free for X_{k-1}, implying that X_{k-1} is a complex and that $f_k \in X_{k-1}$, hence $\hat{f_k} \subseteq X_{k-1}$. Since $X_k = X_{k-1} \setminus \{f_k, g_k\}$ and $g' \neq g_k$, by definition of E_2 we have $(f_k, g') \in E_2$. □

Proposition 11. *Let M be a topological map on X, based on J. Let $s = \min\{M(x) \mid x \in X\}$. If $s < +\infty$, let $t = \min\{M(x) \mid x \in X$ and $M(x) > s\}$, otherwise let $t = +\infty$.*

Then, X collapses onto M_t. Moreover, M (restricted to the elements of M_t) is a topological map on M_t.

Proof. If $s = +\infty$ then the property trivially holds, let us assume $s < +\infty$. Let $S = \{(x_i, y_i)\}_{i=1}^k$ be the set of all pairs of E_1 such that $M(x_i) = M(y_i) = s$. By definition of t, all elements of $X \setminus M_t$ are in these pairs. Let (x, y) be any of these pairs, and let (f_j, g_j) denote the pair of J such that $f_j = y$ and $g_j = x$. We know that $x \subseteq y$.

We claim that (y, x) is free for X. To prove this, suppose that y' is a face of X such that $y' \neq y$ and $x \subseteq y'$. As $(y, x) = (f_j, g_j)$ is free for X_{j-1}, we deduce that there exists a pair (f_ℓ, g_ℓ) in J such that $\ell < j$ and $f_\ell = y'$. Let $x' = g_\ell$. Thus $(x', y') \in E_1$, and by Prop. 10 we have $(y', x) \in E_2$, hence $M(x) > M(y')$, in contradiction with the definition of s and S.

This proves that all pairs (y_i, x_i) in S are free for X. As all these pairs appear in the collapse sequence J, we know that all y_i are distinct faces of X, and by Cor. 2 we conclude that X collapses onto M_t.

The fact that M is a topological map on M_t is a consequence of Cor. 4. □

Th. 12 is a straightforward consequence of Prop. 11.

Theorem 12. *Let M be a topological map on X. Whatever the number $\lambda \in \mathbb{R} \cup \{+\infty\}$, the complex X collapses onto M_λ.*

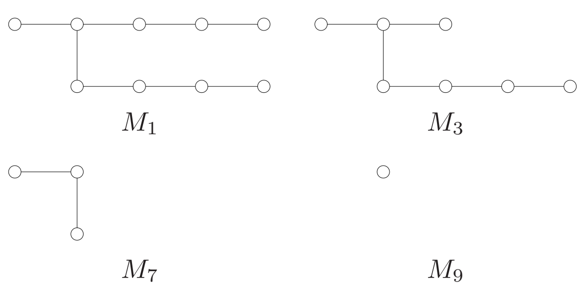

Fig. 11. Level sets of the topological map M of Fig. 10 at levels 1, 3, 7 and 9.

The next theorem (Th. 14) expresses the stability of our skeletonization scheme, with respect to the variations of the filtering parameter.

Let S, T be two subsets of $\mathbb{R}^n$. We set

$$H(S|T) = \max_{s \in S}\{\min_{t \in T}\{d(s,t)\}\},$$

and $d_H(S,T) = \max\{H(S|T), H(T|S)\}$ is the *Hausdorff distance between S and T*.

Let X be a complex in $\mathbb{F}^n$, we denote by $\mathcal{S}(X)$ the union of all faces of X, called the *support of X*. Let X, Y be complexes in $\mathbb{F}^n$, we define the *Hausdorff distance between X and Y* as $d_H(\mathcal{S}(X), \mathcal{S}(Y))$, and we denote it by $d_H(X, Y)$.

The following property follows easily from the definitions.

Proposition 13. *Let Y be a complex, let S be a set of pairs that are free for Y, and let Z be the set of all faces that are in the pairs of Y. Then, $d_H(Y, Y \setminus Z) \leqslant 1$.*

The proof of Th. 14 is quite similar to the one of Prop. 11.

Theorem 14. *Let $\alpha, \lambda \in \mathbb{R}$, $\alpha > 0$, $\lambda \geqslant 0$. Let $k \in \mathbb{N}$. Let M be an α-topological map on X. Then, $d_H(M_\lambda, M_{\lambda + k\alpha}) \leqslant k$.*

Proof. Clearly if the property holds for $k = 1$, it also holds for any k. We assume now that $k = 1$. If $\lambda = +\infty$ then the property trivially holds, let us assume $\lambda < +\infty$. Let $S = \{(x_i, y_i)\}_{i=1}^k$ be the set of all pairs of E_1 such that $\lambda \leqslant M(x_i) = M(y_i) < \lambda + \alpha$. Let (x, y) be any of these pairs, and let (f_j, g_j) denote the pair of J such that $f_j = y$ and $g_j = x$. We know that $x \subseteq y$.

Suppose that y' is a face of M_λ such that $y' \neq y$ and $x \subseteq y'$. As $(y, x) = (f_j, g_j)$ is free for X_{j-1}, we deduce that there exists a pair (f_ℓ, g_ℓ) in J such that $\ell < j$ and $f_\ell = y'$. Let $x' = g_\ell$. Thus $(x', y') \in E_1$, and by Prop. 10 we have $(y', x) \in E_2$, thus $M(x) > M(y') + \alpha$, hence $M(y') < M(x) - \alpha < \lambda$, in contradiction with the fact that y' belongs to M_λ.

This proves that all pairs (y_i, x_i) in S are free for M_λ, and by Prop. 13, we deduce the result. □

7 Topological map induced by an arbitrary map

In this section, we show that given any map L on X, we can define and compute a topological map which is "close to" L, more precisely it is the lowest map over L that is a topological map.

Definition 15. *Let L be any map from X to $\mathbb{R} \cup \{+\infty\}$, and let α be a strictly positive real number. We consider a map M such that:*
a) M is an α-topological map; and
b) for all f in X_J, $M(f) \geqslant L(f)$; and
c) M is minimal for conditions a) and b), that is, any map M' verifying both a) and b) is such that $M' \geqslant M$.

*As stated by the following property, M is uniquely defined. We say that the map M is the α-*topological map induced *by L.*

Proposition 16. *Let M and M' two maps that verify conditions a), b) and c) above. Then, we have $M = M'$.*

Proof. Since for any couple (x, y) of E_1 we have $M(x) = M(y)$ and $M'(x) = M'(y)$, we observe that either M and M' are equal, or they differ on a certain number of couples of E_1. Suppose that (x, y) is a couple of E_1 such that $M'(x) \neq M(x)$. Without loss of generality, we assume that (1) $M'(x) > M(x)$ (hence also $M'(y) > M(y)$), and (2) no face z of X verifies both $M'(z) \neq M(z)$ and $M'(z) < M'(x)$.

Consider the map M'' such that $M''(x) = M''(y) = M(x) = M(y)$, and $\forall z \in X \setminus \{x, y\}$, $M''(z) = M'(z)$. Obviously M'' verifies condition b) above. We claim that M''

is an α-topological map, contradicting the minimality of M'; proving this claim will achieve the proof.

Conditions i) and iii) of Def. 9 are easily verified. Condition ii) must only be checked for arcs adjacent to x and y, since for all other arcs, M'' and M' coincide.

If (z, x) is an arc of E then necessarily $(z, x) \in E_2$. We have $M'(x) \geqslant M'(z) + \alpha$, hence $M'(z) < M'(x)$ and by (2), $M'(z) = M(z)$. We also have $M(x) \geqslant M(z) + \alpha$, and by definition of M'' we deduce $M''(x) \geqslant M''(z) + \alpha$.

If (y, z) is an arc of E then necessarily $(y, z) \in E_2$. We have $M'(z) \geqslant M'(y) + \alpha$. By definition of M'', we know that $M'(z) = M''(z)$ and $M(y) = M''(y)$; and by (1), $M'(y) > M''(y)$. From all this we conclude that $M''(z) \geqslant M''(y) + \alpha$. $\square$

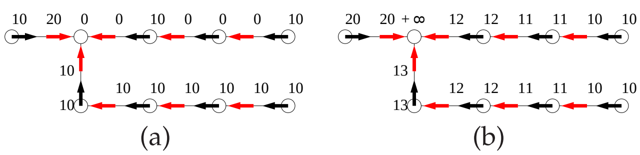

Fig. 12. (a): A map L on the complex X of Fig. 10. (b): The 1-topological map induced by L.

This notion is illustrated in Fig. 12. Below, we give an algorithm that computes the α-topological map induced by any given map on X. Before this, let us recall briefly the notions of rank and topological sort (an introduction to topological sort, including definition, properties and algorithm, can be found *e.g.* in [14]). Let $G = (V, E)$ be an acyclic graph and let $x \in V$, the *rank of* x *in* G is the length of the longest path in G that ends in x. The *topological sort of* G is an operation that results in a partition $\{V^r\}_{r=0}^{r=k}$ of V such that each V^r is the subset of V containing all vertices of rank r.

Algorithm 4: *AlphaTM*(X, E_1, E_2, L, α)

Data: A complex X, the arc sets E_1, E_2 of a flow graph on X, a map L from X to $\mathbb{R}$, a real number $\alpha > 0$

1 **foreach** $x \in X$ **do**
  if x *does not appear in* $E_1 \cup E_2$ **then**
    $M(x) = +\infty$;
  else
    $M(x) = L(x)$;
2 Let $\{X^r\}_{r=0}^{r=k}$ be the result of the topological sort of the acyclic graph $(X, E_1 \cup E_2)$;
3 **for** $r = 0 \rightarrow k$ **do**
4   **foreach** $x \in X^r$ **do**
5   **foreach** y *such that* $(y, x) \in E_1$ **do**
        $M(y) = M(x) = \max\{M(x), M(y)\}$;
6   **foreach** y *such that* $(y, x) \in E_2$ **do**
        $M(x) = \max\{M(x), M(y) + \alpha\}$;
7 **return** M;

Proposition 17. *Let M be a map from X to $\mathbb{R}$, and let α be real number, $\alpha > 0$. The result of AlphaTM(X, E_1, E_2, M, α) is the α-topological map induced by M.*

Proof. Condition iii) of Def. 9 is ensured by line 1. In lines 3-6, each vertex of the flow graph is examined exactly once, and, due to the order of scanning (lines 3,4) and by definition of topological sort, the final values $M(y)$ of all predecessors y of the current vertex x have been computed before it is examined. For vertices that have no predecessor, the output value of M is equal to the input value. Otherwise, lines 5 and 6 ensure that conditions i) and ii') of Def. 9 hold. By construction, the minimality of M is guaranteed. $\square$

Let N_v denote the number of vertices, and N_a the number of arcs of the graph $(X, E_1 \cup E_2)$. The time complexity of the above algorithm is in $O(N_v + N_a)$.

8 Computing hierarchic skeletons

Let us now summarize our method to produce families of filtered homotopic skeletons of any complex X in $\mathbb{F}^n$ (see algorithm 5).

Algorithm 5: *TopoMap*(X, L, α)

Data: A complex X, a map L on X, a real number α

Let P be the projection radius map of X (see Sec. 3);
Let $J =$ *GuidedCollapse*(X, P) (see Sec. 4);
Let $(X, E = E_1 \cup E_2)$ be the flow graph associated to J, and let Γ, Γ^{-1} be the successor and predecessor functions of this graph (see Sec. 4);
Let $\widetilde{L} =$ *Integrate*$(X, \Gamma, \Gamma^{-1}, L)$ (see Sec. 5);
Let $M =$ *AlphaTM*$(X, E_1, E_2, \widetilde{L}, \alpha)$ (see Sec. 6);
return M;

First, we compute the projection radius map (Sec. 3) on the d-faces of X, and extend it to other elements of X (if $y \in X$ is not an d-face, then we set $P(y)$ to the max of $P(x_i)$ where the x_i's are all d-faces that contain y).

Using algorithm 1 (Sec. 4) we build a collapse sequence and a flow graph on X.

By construction, the upstream (Sec. 5) of any vertex x of this flow graph is composed by elements of X that, in any family of filtered skeletons, should disappear before x does.

Integrating information given by map L (Sec. 5) allows us to associate, to each element x of X, a value $\widetilde{L}(x)$ that represents a measure of the upstream of x. The lower this value, the sooner the point x may disappear.

Then, thanks to algorithm 4 (Sec. 6), we produce a topological map M based on this measure. Thanks to Th. 12, we know that any level set of M is homotopy-equivalent to X.

Some results are shown in Fig. 13 and Fig. 14, using map L_2.

Another interesting map is L_3, which associates to each point x of X the bisector angle of x, that is, the

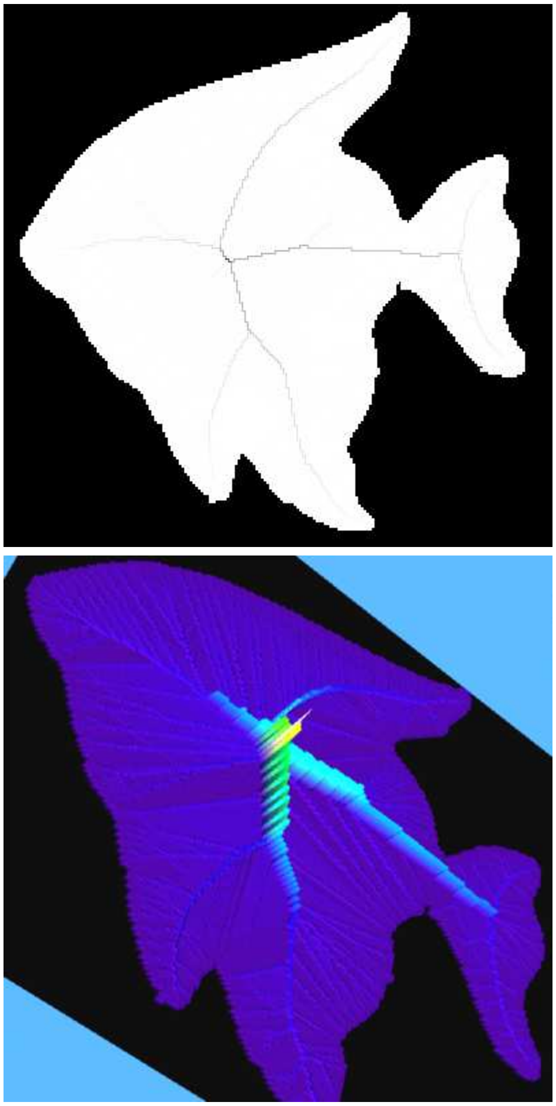

Fig. 13. Two renderings of the result of the *TopoMap* operator, on the same object X as in Fig. 5 and the map $L_2 = 1_{B(X)}$.

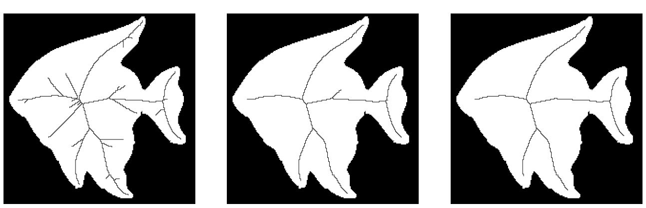

(a) (b) (c)

Fig. 14. (a,b,c): Three level sets of $\mathit{TopoMap}(X, L_2)$, at values 25, 48 and 72 respectively.

maximal angle $\widehat{axb}$ with a, b any two points in the extended projection of x on $\overline{X}$ (see [15]). In the next section, we will see that L_3 yields particularly good results.

9 Quality assessment and comparisons

In order to assess the quality of the produced skeletons, and to compare them to those obtained by other methods, we use stability w.r.t. rotations as our quality criterion, following a methodology introduced in [11].

Rotation invariance is an important property of skeleton that holds in the continuous framework. If R_θ denotes the rotation of angle θ and center 0, and S denotes the skeleton transform, the rotation invariance property states that $S(R_\theta(X)) = R_\theta(S(X))$, whatever X and θ.

In a discrete framework, this property can only hold for particular cases (*e.g.*, when θ is a multiple of 90 degrees). Nevertheless, we can experimentally measure the dissimilarity between $S(R_\theta(X))$ and $R_\theta(S(X))$ for different instances of X and θ, and different definitions of skeleton. The lower this dissimilarity, the more stable under rotation the method is.

Let us now describe more precisely the methodology that we used for this experimental evaluation.

Let X be a finite subset of $\mathbb{Z}^n$. Notice that a cubical complex has a natural embedding in $\mathbb{Z}^n$ and can thus be treated as a point set. Let $Y \subseteq X$, we set $RDT_X(Y) = \bigcup_{y \in Y} B^<_{d(y,\overline{X})}(y)$, where $B^<_r(x) = \{y \in \mathbb{Z}^n \mid d(x,y) < r\}$. The transformation RDT_X is sometimes called *reverse distance transform* [13].

It is well known that any object can be fully reconstructed from its medial axis, more precisely, we have $X = RDT_X(Y)$ whenever Y is the the set of all centers of maximal balls of X. However, this is no longer true if we consider filtered skeletons.

Then, it is interesting to measure how much information about the original object is lost when we raise the filtering parameter. Considering a skeletonization procedure S_λ where λ is the only parameter, we set

$$\rho_X(\lambda) = \frac{|X \setminus RDT_X(S_\lambda(X))|}{|X|}.$$

In words, $\rho_X(\lambda)$ is the area of the difference between X and the set reconstructed from its filtered skeleton, divided by the area of X. We call $\rho_X(\lambda)$ the *(normalized) residual (of X, corresponding to filtering value λ)*.

Obviously, for different skeletonization methods the filtering parameter does not play the same role. To ensure a fair evaluation we will compare the results of different methods for approximately equal values of their residuals, rather than for equal values of their parameters.

For comparing shapes or skeletons, we use the Hausdorff distance (see Sec. 6), and also a dissimilarity measure proposed by M.P. Dubuisson and A.K. Jain [17] as an alternative to the Hausdoff distance. The drawback of Hausdorff distance for measuring shape dissimilarity is its extreme sensibility to outliers, the latter measure avoids this drawback.

Let X, Y be two subsets of $\mathbb{R}^n$. We set

$$D(X|Y) = \frac{1}{|X|} \sum_{x \in X} \min_{y \in Y} \{d(x,y)\},$$

and $d_D(X,Y) = \max\{D(X|Y), D(Y|X)\}$ is the *Dubuisson and Jain's dissimilarity measure between X and Y* (called *dissimilarity* in the sequel for the sake of brevity).

We conducted our experiments on a database of 216 shapes provided by B.B. Kimia [31]. The 216 images are divided into 18 classes (birds, cars, etc.), Fig. 15 shows one (reduced) image of each class.

Fig. 15. A sample of the 216 shapes of Kimia's database.

In those experiments, we compare three variants of our method, and two other methods which are, to the best of our knowledge, among the best ones in regard to the stability criterion which is our main concern in this work. More precisely, we compare:
a) Our method, using the map L_1 as described in section 5 (area indicator);
b) Our method, using the map L_2 as described in section 5 (border indicator);
c) Our method, using the map L_3 as described in section 5 (bisector angle);
d) A homotopic thinning procedure by iterative simple point removal, guided by a priority function which is the PR map, and constrained to preserve the points belonging to the λ-medial axis;
e) The skeletonization method proposed by R. Ogniewicz, using the implementation that can be found in the Stony Brook Algorithm Repository[1].

	1%	2%	3%	4%	5%	6%	all
a	1.22	1.58	1.69	1.63	1.53	1.46	1.52
b	1.67	1.87	1.48	1.23	1.24	1.29	1.46
c	1.56	1.69	1.44	1.20	1.10	1.09	1.35
d	2.23	1.57	1.32	1.24	1.28	1.34	1.50
e	1.78	1.78	1.45	1.16	1.09	1.05	1.39

TABLE 1
Dissimilarity

Tables 1 and 2 show respectively average dissimilarity and Hausdorff distance between $S(R_\theta(.))$ and $R_\theta(S(.))$, on all shapes of the database, for angles θ varying between 0 and 89 degrees by steps of one degree, and for applications of the five methods yielding residuals varying between 1% and 6%. Fig. 16 illustrate the level of filtering obtained on a shape for these residual values.

1. http://www.cs.sunysb.edu/~algorith/implement/skeleton/implement.shtml

	1%	2%	3%	4%	5%	6%	all
a	7.80	11.7	13.7	14.4	14.0	13.4	12.5
b	14.0	17.6	14.7	11.0	9.83	9.83	12.8
c	12.6	15.4	14.0	10.9	8.59	7.99	11.6
d	16.6	15.9	13.7	12.8	12.7	12.6	14.1
e	14.6	15.1	13.2	9.48	7.95	7.19	11.3

TABLE 2
Hausdorff distance

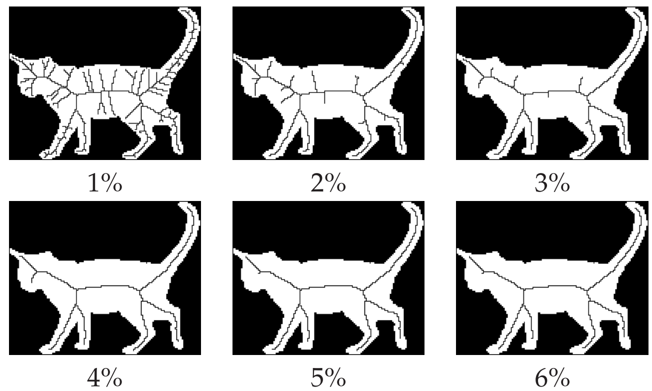

Fig. 16. Filtered skeletons (method b) yielding 1% to 6% residuals.

It can be observed that variant (a) of our method performs very well with moderate filtering, while for higher residual amounts Ogniewicz' method (e) is best. In the average, variant (c) of our method performs as well as (e).

10 The 3D case

Unlike former approaches to define and compute hierarchic or multiscale skeleton, our method also applies to 3D objects. All definitions and algorithms that we gave previously are indeed valid whatever the dimension of the complex. We illustrate this by showing a few results in 3D: see Fig. 17.

11 Conclusion

The method that we propose is guaranteed to preserve topology and is stable with respect to variations of the filtering parameter, as stated by Th. 12 and Th. 14 respectively. We compared it (in 2D) with the method of [26] and with a topology-preserving method directly based on the DLMA, regarding the stability w.r.t. rotations. This comparison is in favour of our method, as reported in Sec. 9. We also illustrate in Sec. 10 its application in 3D for obtaining curvilinear skeletons. Furthermore, our method is highly flexible: many variants can be imagined, in particular by choosing alternative valuations of the upstream. In further works, we will investigate the case of 3D surface skeletons, and the possibility to obtain skeletons only composed of voxels.

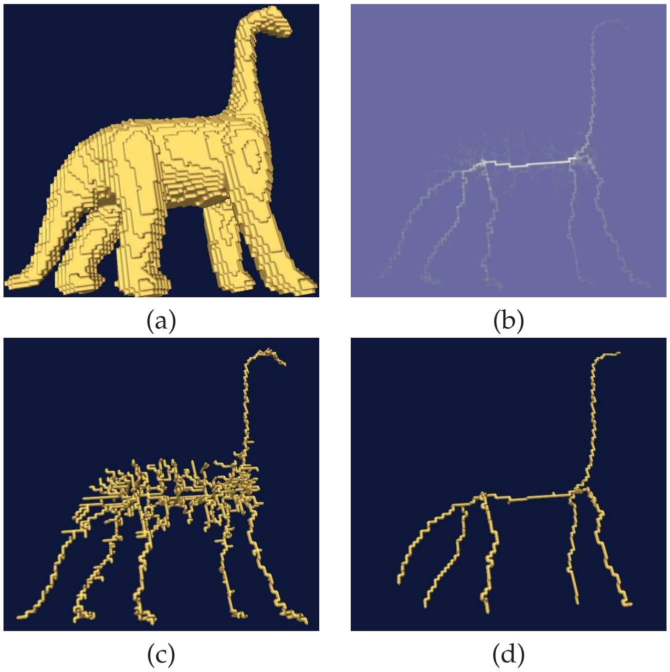

Fig. 17. (a): Original shape X. (b): Topological map M induced by $L_2(X)$. (c): The level set M_{100}, a skeleton of X. (d): The level set M_{1200}, another skeleton of X.

REFERENCES

[1] D. Attali, J.-D. Boissonnat, and H. Edelsbrunner. Stability and computation of the medial axis — a state-of-the-art report. In T. Möller, B. Hamann, and B. Russell, editors, *Mathematical Foundations of Scientific Visualization, Computer Graphics, and Massive Data Exploration*, pages 1–19. Springer-Verlag, 2009. to appear.

[2] D. Attali and J.O. Lachaud. Delaunay conforming iso-surface, skeleton extraction and noise removal. *Computational Geometry: Theory and Applications*, 19:175–189, 2001.

[3] D. Attali and A. Montanvert. Modelling noise for a better simplification of skeletons. In *Procs. International Conference on Image Processing (ICIP)*, volume 3, pages 13–16, 1996.

[4] Dominique Attali, Gabriella Sanniti di Baja, and Edouard Thiel. Pruning discrete and semicontinuous skeletons. In *Procs. Conf. Image Analysis and Processing*, volume 974 of *Lecture Notes in Computer Science*, pages 488–493. Springer, 1995.

[5] Xiang Bai, Longin Jan Latecki, and Wen-Yu Liu. Skeleton pruning by contour partitioning with discrete curve evolution. *Transactions on Pattern Analysis and Machine Intelligence*, 29(3):449–462, 2007.

[6] G. Bertrand and M. Couprie. Two-dimensional parallel thinning algorithms based on critical kernels. *Journal of Mathematical Imaging and Vision*, 31(1):35–56, 2008.

[7] Gilles Bertrand and Michel Couprie. A new 3D parallel thinning scheme based on critical kernels. In *Discrete Geometry for Computer Imagery*, volume 4245 of *Lecture Notes in Computer Science*, pages 580–591. Springer, 2006.

[8] H Blum. A transformation for extracting new descriptors of shape. In W Wathendunn, editor, *Models for the Perception of Speech and Visual Form*, pages 362–380. MIT Press, 1967.

[9] G. Borgefors, I. Ragnemalm, and G. Sanniti di Baja. The Euclidean distance transform: finding the local maxima and reconstructing the shape. In *Procs. of the 7th Scandinavian Conference on Image Analysis*, volume 2, pages 974–981, 1991.

[10] John Chaussard and Michel Couprie. Surface thinning in 3D cubical complexes. In *13th International Workshop on Combinatorial Image Analysis (IWCIA'09)*, LNCS, pages 1–12, 2009. To appear.

[11] John Chaussard, Michel Couprie, and Hugues Talbot. A discrete lambda-medial axis. In *15th Discrete Geometry for Computer Imagery (DGCI'09)*, Lecture Notes in Computer Science, pages 1–12, 2009. To appear.

[12] F. Chazal and A. Lieutier. The lambda medial axis. *Graphical Models*, 67(4):304–331, 2005.

[13] D. Coeurjolly. d-dimensional reverse Euclidean distance transformation and Euclidean medial axis extraction in optimal time. In *procs. DGCI, LNCS, Springer Verlag*, volume 2886, pages 327–337, 2003.

[14] T. H. Cormen, C. Leiserson, and R. Rivest. *Introduction to algorithms*. MIT Press, 1990.

[15] Michel Couprie, David Coeurjolly, and Rita Zrour. Discrete bisector function and Euclidean skeleton in 2D and 3D. *Image and Vision Computing*, 25(10):1543–1556, 2007.

[16] E.R. Davies and A.P.N. Plummer. Thinning algorithms: a critique and a new methodology. *Pattern Recognition*, 14:53–63, 1981.

[17] M.-P. Dubuisson and A.K. Jain. A modified Hausdorff distance for object matching. In *Proceedings of the 12th IAPR International Conference on Pattern Recognition*, volume 1, pages 566–568, 1994.

[18] A.X. Falcao, L. da Fontoura Costa, and B.S. da Cunha. Multiscale skeletons by image foresting transform and its application to neuromorphometry. *Pattern Recognition*, 35(7):1571–1582, 2002.

[19] Robin Forman. Morse theory for cell complexes. *Advances in mathematics*, 134(1):90–145, 1998.

[20] Y. Ge and J.M. Fitzpatrick. On the generation of skeletons from discrete Euclidean distance maps. *IEEE Transactions on Pattern Analysis and Machine Intelligence*, 18(11):1055–1066, 1996.

[21] Wim H. Hesselink and Jos B.T.M. Roerdink. Euclidean skeletons of digital image and volume data in linear time by the integer medial axis transform. *IEEE Transactions on Pattern Analysis and Machine Intelligence*, 30(12):2204–2217, 2008.

[22] A. Lieutier. Any open bounded subset of $\searrow^n$ has the same homotopy type as its medial axis. In *Proc. 8th ACM Symposium on Solid Modeling Applications*, pages 65–75. Academic Press, 2003.

[23] L. Liu, E. Chambers, D. Letscher, and T. Ju. A simple and robust thinning algorithm on cell complexes. In *Proceedings of Pacific Graphics 2010*, Computer Graphics Forum, pages 1–8, 2010. to appear.

[24] G. Malandain and S. Fernández-Vidal. Euclidean skeletons. *Image and Vision Computing*, 16:317–327, 1998.

[25] G. Matheron. *Examples of topological properties of skeletons*, volume 2, pages 217–238. Academic Press, 1988.

[26] R.L. Ogniewicz and O. Kübler. Hierarchic Voronoi skeletons. *Pattern Recognition*, 28(33):343–359, 1995.

[27] M. Pierrot-Deseilligny, G. Stamon, and C.Y. Suen. Veinerization: a new shape description for flexible skeletonization. *IEEE Transactions on Pattern Analysis and Machine Intelligence*, 20(5):505–521, 1998.

[28] C. Pudney. Distance-ordered homotopic thinning: a skeletonization algorithm for 3D digital images. *Computer Vision and Image Understanding*, 72(3):404–413, 1998.

[29] E. Rémy and E. Thiel. Exact medial axis with Euclidean distance. *Image and Vision Computing*, 23(2):167–175, 2005.

[30] J. Serra. *Image analysis and mathematical morphology*. Academic Press, 1982.

[31] D. Sharvit, J. Chan, H. Tek, and B.B. Kimia. Symmetry-based indexing of image databases. *Journal of Visual Communication and Image Representation*, 9(4):366–380, 1998.

[32] K. Siddiqi, S. Bouix, A. Tannenbaum, and S. Zucker. The Hamilton-Jacobi skeleton. In *International Conference on Computer Vision (ICCV)*, pages 828–834, 1999.

[33] P. Soille. *Morphological image analysis*. Springer-Verlag, 1999.

[34] Stina Svensson and Gabriella Sanniti di Baja. Simplifying curve skeletons in volume images. *Computer Vision and Image Understanding*, 90(3):242–257, 2003.

[35] H. Talbot and L. Vincent. Euclidean skeletons and conditional bisectors. In *Procs. VCIP'92, SPIE*, volume 1818, pages 862–876, 1992.

[36] L. Vincent. Efficient computation of various types of skeletons. In *Procs. Medical Imaging V, SPIE*, volume 1445, pages 297–311, 1991.

[37] J.H.C. Whitehead. Simplicial spaces, nuclei and m-groups. *Proceedings of the London Mathematical Society*, 45(2):243–327, 1939.